Journal of Geoscience and Environment Protection, 2023, 11, 293-304
https://www.scirp.org/journal/gep
ISSN Online: 2327-4344
ISSN Print: 2327-4336

Overbank Flow in a Multi-Staged Open Channel: Zonal and Overall Discharge Studies

Prateek Kumar Singh[1,2], Xiaonan Tang[2], Hamidreza Rahimi[3], Yutong Guan[2]

[1]Department of Building Environment and Energy Engineering, Hong Kong Polytechnic University, Hong Kong, China
[2]Department of Civil Engineering, Xi'an Jiaotong Liverpool University, Suzhou, China
[3]State Key Laboratory of Hydrology-Water Resources and Hydraulic Engineering, Hohai University, Nanjing, China
Email: prateek.singh@polyu.hk

How to cite this paper: Singh, P. K., Tang, X. N., Rahimi, H., & Guan, Y. T. (2023). Overbank Flow in a Multi-Staged Open Channel: Zonal and Overall Discharge Studies. *Journal of Geoscience and Environment Protection, 11,* 293-304.
https://doi.org/10.4236/gep.2023.113016

Received: January 28, 2023
Accepted: March 28, 2023
Published: March 31, 2023

Abstract

An improved divided channel method has been proposed by modelling a parameter using the function of depth ratio for a multi-stage compound channel. Experimental data suggest that as the flow depth increases over the second stage floodplain, fractional contribution of the main channel and first stage floodplain under bankfull height plays a pivotal role in shear layer and momentum distribution. Therefore, a new mathematical model has been suggested for estimating the stage-discharge relationship for staged channels of more than one floodplain using the 1D technique of overall roughness correction.

Keywords

Overbank Floodplains, River Dynamics, Asymmetric Channels, Open-Channel Flows

1. Introduction

Numerous overtopping and high-flow events suggest different cross-sectional land characteristics of the river and urban river water systems. The understanding of overbank flows in compound open channels, which have a deeper main channel and distinct floodplains with differential bankfull heights (multi-stage floodplains), is of primary importance. Multi-stage compound channels are viable in urban areas to facilitate bank slope stability and higher discharge capacity for different flow rates (Wang et al., 2014; Chen et al., 2019). The complexity of the multi-stage compound channels manifolds with interactive geometry and roughness of the surrounding floodplains. In the present study, a comprehensive experimental analysis is conducted to understand the flow at the different interfaces of such channels. This paper presents an experimental investigation of the effect on the momentum flux at individual contiguous staged floodplains. Moreover, zonal and overall discharge are illustrated using the 1D analytical analysis to estimate the improved divided channel method and flow resistance proposition.

2. Methodology

2.1. Experimental Arrangements

The experiments were performed in a 20 m long and 0.745 m wide glassed-wall flume in the Hydraulic Laboratory of Xi'an Jiaotong-Liverpool University (XJTLU), China. The compound channel cross-section was rectangular, with the main channel width (b_c) of 0.445 m, first-stage floodplain width (b_{f1}) of 0.1 m, and second-stage floodplain width (b_{f2}) of 0.2 m (see **Figure 1(a)**). The longitudinal bottom slope of the flume was $S_o = 0.003$. The floodplains were covered with flexible plastic grass turf, whose density was 33,000 grass blades/cm^2 and whose blade height was 8.3 mm. The bankfull height (h_i) was 4 cm for the

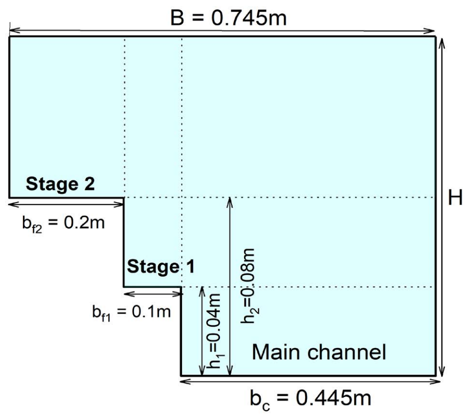

(a)

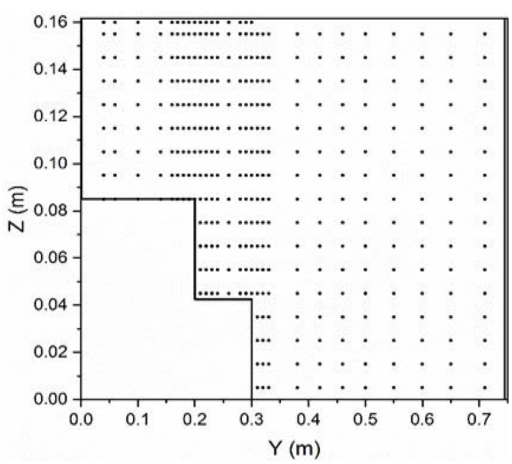

(b)

Figure 1. Multi-stage compound channel: (a) cross-section, with two floodplain widths, and (b) cross-sectional measurement location for ADV.

first-stage floodplain (i = 1) and 8 cm for the second-stage floodplain (i = 2). With the dual existence of the interfacial section and bankfull height, the relative depth ratio D_r (the flow depth above the floodplain/main channel depth) was variable at each stage distinctively. The flow analysis in this study is based on $h_2 = 8$ cm. The measurement cross-section was located 11 m from the entrance of the flume. The x-, y-, and z-axes refer to the streamwise (along the flume), transverse and vertical (normal to the bed) directions, respectively. In this Cartesian coordinate system, the instantaneous velocities, time-averaged velocities, and velocity fluctuations are denoted as (u_x, u_y, u_z), (U_x, U_y, U_z) and (u'_x, u'_y, u'_z) respectively. Five flow depths were investigated in the range of $0.1 \le D_r \le 0.5$.

2.2. Measurements

Figure 1(b) shows the measuring location of the cross-section with a lateral interval of 0.01 m near the interface and 0.05 - 0.02 m in other areas. Contrary to the lateral spacing, vertical spacing was 0.01 m from the bottom to the free surface. Velocity was measured using 3-D Nortek Vectrino side and down-looking acoustic Doppler velocimetry (ADV), which has a sampling volume 5 cm away from the probe. At each measuring point, the three instantaneous velocity components were recorded at 200 Hz for 180 - 300 s (more time near the interface) with a signal-to-noise ratio greater than 18 - 20 and a no less than 75% correlation rate.

3. Experimental Results

Figure 2 shows the cross-sectional distribution of the mean streamwise velocity (U_x) at three different flow depths (Dr) of 0.1, 0.3, and 0.5. The maximum velocity is located beneath the free surface in the main channel section ($0.3 \le Y \le 0.745$). For the lower flow depth (Dr = 0.1), the significant change of velocity over the three stages of the compound section suggests a strong mixing layer, especially between stage one ($0.2 \le Y \le 0.3$) and stage two ($0 \le Y \le 0.2$). The velocities in stages one and two decelerate due to low momentum transport caused by the secondary current.

Momentum Flux Distribution at the Interface

The momentum flux distribution is shown in **Figures 3(a)-(e)** through the distribution of transverse velocity U_y, indicating the presence of transverse currents from the main channel towards the floodplains. The degree of flow anisotropy is measured by σ_z/σ_x, where $\sigma_z = \sqrt{\overline{u'_z u'_z}}$ and $\sigma_x = \sqrt{\overline{u'_x u'_x}}$ are the standard deviations of the vertical and streamwise velocities, respectively. The anisotropy induced at the different stages of interfaces is shown in **Figures 4(a)-(e)** at the different spanwise locations of the multi-stage compound channels.

For the same flow, two transverse profiles of U_y in **Figure 3(b)** and **Figure 3(d)** reveal the development of secondary currents persistently near the stage $y_{int=2} = 20$ cm and $y_{int=1} = 30$ cm, termed as longitudinal vortex (Tominaga

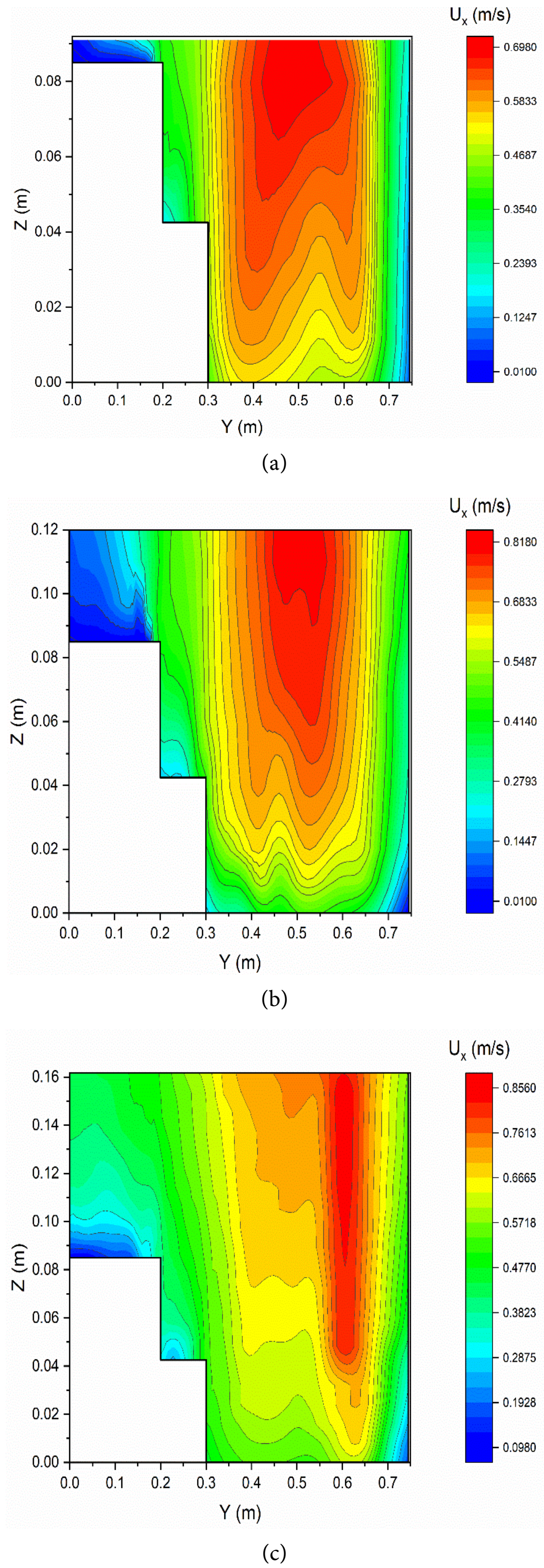

Figure 2. Contour mapping of the streamwise velocity for (a) $Dr = 0.1$, (b) $Dr = 0.3$, and (c) $Dr = 0.5$.

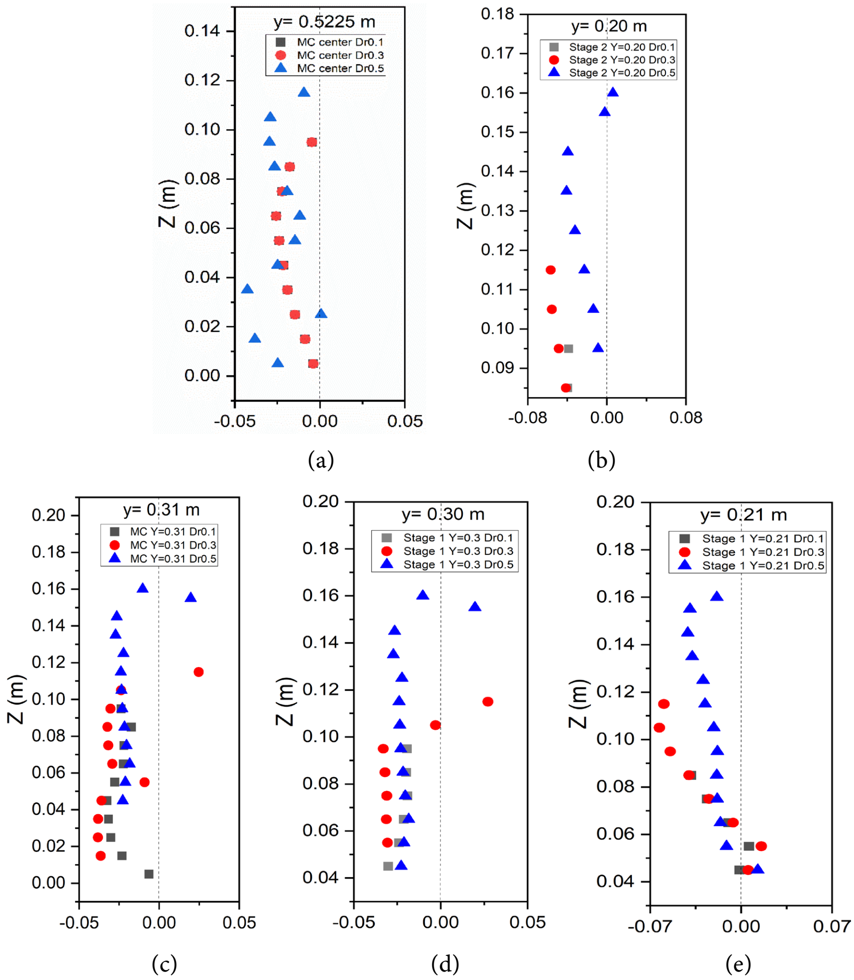

Figure 3. Vertical distributions of the time-averaged transverse velocity U_y over the (a) half of the main channel; (b) main channel and stage 1 interface y = 31 cm; (c) at $y_{int=1} = 30$ cm; (d) stage one and two interfaces y = 21 cm; and at $y_{int=2} = 20$ cm for three Dr = 0.1, 0.3 & 0.5 of the multi-stage compound channel flows.

and Nezu, 1991). The same trend is depicted in **Figure 4**, which has spikes of the anisotropy at the bankfull height of Z = 0.4 m and Z = 0.8 m. Furthermore, the greater extent of anisotropy value near the free surface $Z \geq 0.8$ in **Figures 4(c)-(e)** indicates that the presence of large cells extends over the entire flow depths. Tominaga and Nezu (1991) concluded that the secondary currents were more driven by the cross-sectional topography (i.e. by Dr) rather than roughness. However, Proust and Nikora (2020) showed that the strength of the floodplain longitudinal vortex is stronger for $Dr = 0.2$ and rough channels compared to the smooth channels. In this respect, the present data show that the ratio of U_y / U_x is the highest for the second stage floodplains ($0 \leq Y \leq 0.2$), depicting the strongest longitudinal vortex. In addition, for the lower depth ratio $Dr \leq 0.3$, longitudinal vortexes are still visible for the floodplains, which suggests that the wall roughness plays a role in the emergence of the floodplain's secondary cell for lower Dr (Proust and Nikora, 2020).

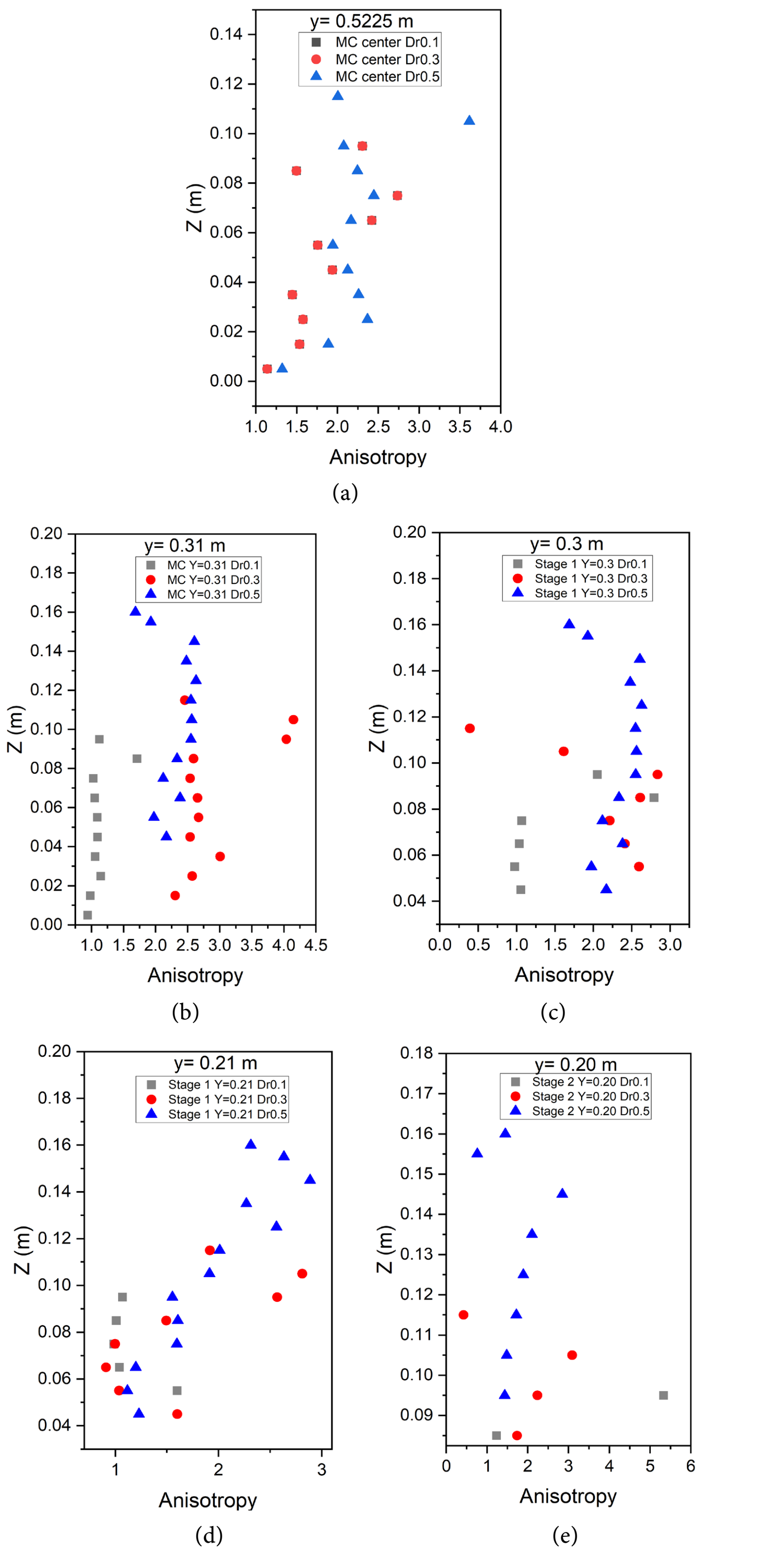

Figure 4. Vertical distributions of the time-averaged transverse anisotropy (σ_z/σ_x) over the (a) half of the main channel; (b) main channel and stage 1 interface $y = 31$ cm; (c) at $y_{int=1} = 30$ cm; (d) stage one and two interfaces $y = 21$ cm; and at $y_{int=2} = 20$ cm for *Dr* = 0.1, 0.3 & 0.5 of the multi-stage compound channel flows.

4. 1D Analytical Solution for a Zonal and Overall Discharge

The channel geometry, as depicted in **Figure 5**, consists of three sections: the main channel (1), the first stage (2), and the second stage (3). The experimental data suggest the existence of different scales of the mixing layer and longitudinal vortex at distinct stages of floodplains. Thus, the destabilizing shear between sections needs to be remodelled using the difference of squared velocities. The streamwise component of shear stress acting along the wetted perimeter on the left-hand and right-hand sides and shear force along with the vertical interfaces are shown in Equations (1)-(3), similar to the methods reviewed by Tang (2016).

$$\rho g A_1 S_o = P_1 \tau_1 + h_{12} \tau_{12a} \tag{1}$$

$$\rho g A_2 S_o = P_2 \tau_2 - h_{12} \tau_{12a} + h_{23} \tau_{23a} \tag{2}$$

$$\rho g A_3 S_o = P_3 \tau_3 - h_{23} \tau_{23a} \tag{3}$$

Let,

$$\tau_i = \rho f_i U_i^2 (i = 1,2,3)\,; \quad \tau_{12a} = \frac{1}{2} \rho \alpha_{12} (U_1^2 - U_2^2)\,; \quad \tau_{23a} = \frac{1}{2} \rho \alpha_{23} (U_2^2 - U_3^2) \tag{4}$$

$$U_{i,o}^2 = \frac{g R_i S_o}{f_i} (i = 1,2,3)\,; \text{ e.g. } U_{1,0}^2 = \frac{g R_1 S_o}{f_1} = \frac{g A_1 S_o}{P_1 f_1} \tag{5}$$

(calculation using divided channel method with vertical divisions and without interaction)

4.1. Improved Divided Channel Method (IDCM) for Multi-Stage Channels

The apparent shear stress acting on the imaginary interface (h_i) is scaled using squared flow velocities in Equation (4), as shown by Huthoff et al. (2008), Tang (2017), Tang (2019a, 2019b), Singh et al. (2019), and Singh and Tang (2020). The shear stress that slows down the main channel flow is exactly the opposite of the stress that accelerates the flow in the floodplain(s), thus explaining minus sign in Equations (2) and (3). Applying the interacting divided channel method (IDCM) to the multi-stage channel geometries depicted in **Figure 5** requires solving Equations (1)-(5), which give:

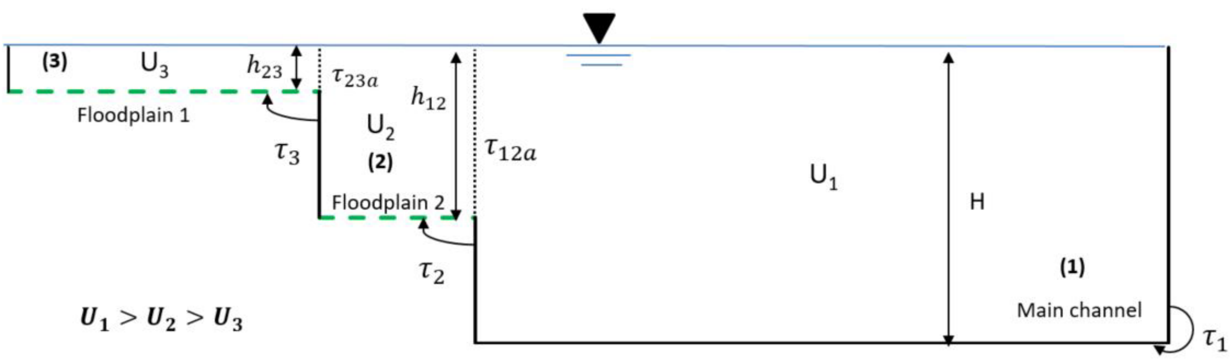

Figure 5. Cross-section of a multi-stage channel with one main channel and two stages of the floodplain. The vertical dashed lines show the interfaces between subsections.

$$U_1^2 = \frac{[(1+\alpha_{12}\varepsilon_{12})(1+\alpha_{23}\varepsilon_3)+\alpha_{23}\varepsilon_{23}]U_{1,0}^2 + (\alpha_{12}\varepsilon_1)(1+\alpha_{23}\varepsilon_3)U_{2,0}^2 + (\alpha_{12}\varepsilon_1)(\alpha_{23}\varepsilon_{23})U_{3,0}^2}{(1+\alpha_{12}\varepsilon_1)\alpha_{23}\varepsilon_{23} + (1+\alpha_{12}\varepsilon_1+\alpha_{12}\varepsilon_{12})(1+\alpha_{23}\varepsilon_3)} \quad (6)$$

$$U_2^2 = \frac{1}{\alpha_{12}\varepsilon_1}[(1+\alpha_{12}\varepsilon_1)U_1^2 - U_{1,0}^2] = U_1^2 + \frac{1}{\alpha_{12}\varepsilon_1}(U_1^2 - U_{1,0}^2) \quad (7)$$

$$U_3^2 = \frac{1}{1+\alpha_{23}\varepsilon_3}[U_{3,0}^2 + \alpha_{23}\varepsilon_3 U_2^2] \quad (8)$$

$$\varepsilon_1 = \frac{h_{12}}{2P_1 f_1};\quad \varepsilon_{12} = \frac{h_{12}}{2P_2 f_2};\quad \varepsilon_{23} = \frac{h_{23}}{2P_2 f_2};\quad \varepsilon_3 = \frac{h_{23}}{2P_3 f_3} \quad (9)$$

4.2. New Parameter α_{ij} for Zonal Discharge Comparative Analysis

The dimensionless parameters in Equations (6)-(8) are given in Equation (9), where interfacial height (h_i), wetted perimeter (P_i) and friction factor (f_i) are designated for individual sections, as shown in **Figure 5**. The solutions are presented in terms of flow velocities obtained by correcting the divided channel method (DCM), where interface stress is neglected (i.e. take α_{12} and α_{23} as zero). However, in the following analysis, α_{12} and α_{23} are estimated for the multi-stage compound channels with roughness, which can be specified as either manning's *n* or friction factor *f*.

Figure 6(a) shows the vertical interface coefficient α_{ij} of the apparent shear stress in Equations (6)-(8) for the range of $0.1 \le Dr \le 0.5$. The data points in **Figure 6(a)** suggest functions of α_{ij} with *Dr* for individual cases of RR(20)304. Value of the α_{ij} for IDCM and IDCM-new is given in **Table 1**. Huthoff et al. (2008) and Yang et al. (2014) presented these coefficients as 0.02 and 0.04 for single-staged compound open channel flow, respectively.

To examine the performance of the three models: DCM, IDCM, and IDCM-new, the absolute relative error percentage of the predicted discharge is presented in **Table 1**.

$$\%\,error = \frac{\left|Q_{cal.i} - Q_{exp,i}\right|}{Q_{exp,i}} \times 100\% \quad (10)$$

where $\%\,error$ is the relative error percentage of the predicted and observed discharge at i_{th} flow depth, respectively. **Figure 6(b)** shows the five-depth ratio's experimental zonal discharge and the predicted discharge. DCM and IDCM

Table 1. Functions for α_{ij} as a function of *Dr* for different floodplain widths.

Case	Model		
	DCM	IDCM	IDCM-new
α_{12}	-	0.02	$0.0187Dr^2 - 0.2332Dr + 0.8821$
α_{23}	-	0.02	$4.1518Dr^2 - 2.9748Dr + 0.5395$
% error	42.9	18.0	4.2

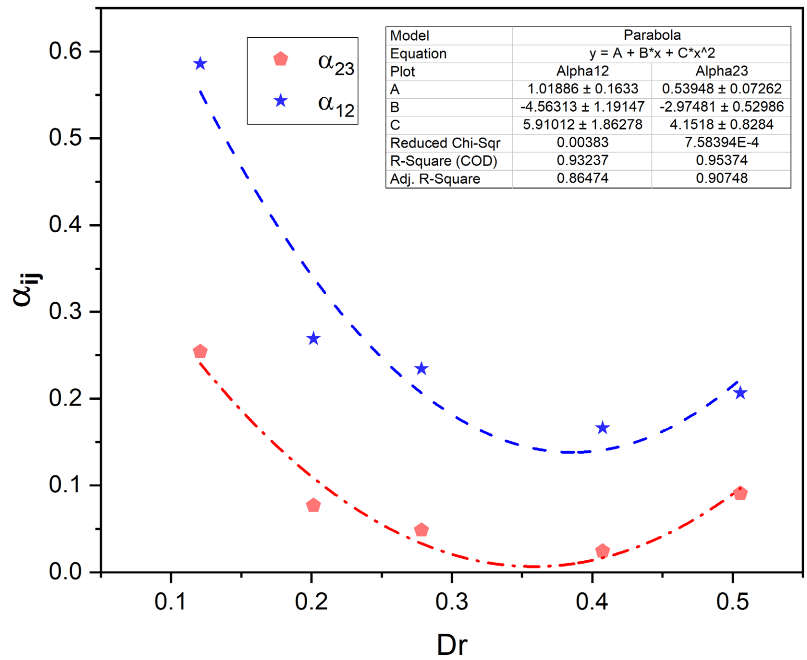

(a)

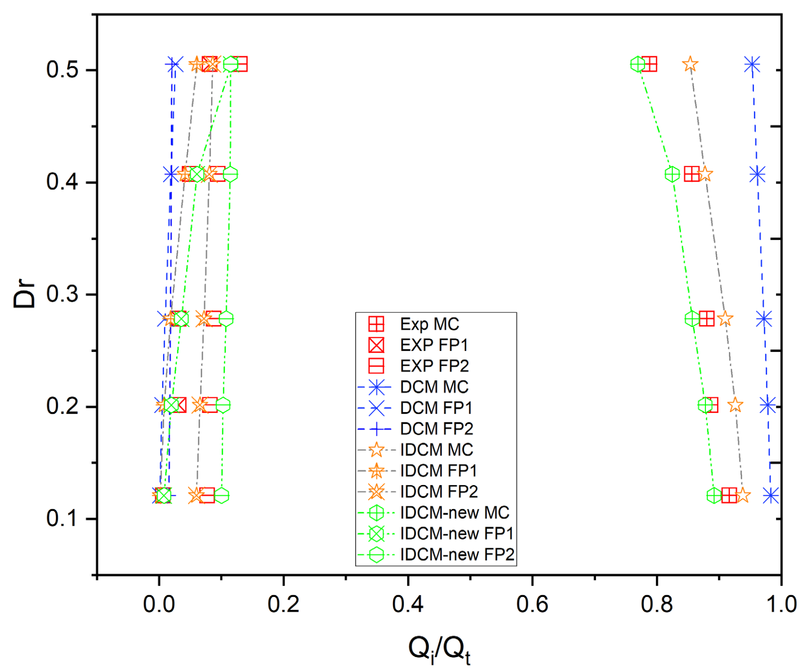

(b)

Figure 6. (a) Correlation of the coefficient α_{ij} of apparent shear friction on the vertical interface with *Dr* for experimental data. (b) Comparison of normalized zonal discharge (Q_i/Q_t) for all the data, including main channel (MC), floodplain 1 (FP1 with $y_{int=2}$ at 20 cm) and floodplain 2 (FP2 with $y_{int=1}$ at 30 cm) discharge.

methods overestimate the main channel (MC), stage 1 ($y_{int=2}$ at 20 cm) and stage 2 ($y_{int=1}$ at 30 cm) discharges for all depth ratios. IDCM-new underestimates the minor errors for all three sections of the compound channel, including lower depth ratios. The estimation of zonal discharge for floodplain 1 ($y_{int=2}$ at 20 cm) and floodplain 2 ($y_{int=1}$ at 30 cm) is well predicted with minor errors using the new coefficient α_{ij} .

4.3. Study of Flow Resistance in the New Configuration of Asymmetric Channels

Traditionally, flow resistance plays a pivotal role in using a simple 1D method to estimate stage discharge. However, it has been pointed out by Cao et al. (2006) that the estimation of flow resistance experiences significant uncertainty and needs more accurate approaches. To formulate depth-averaged velocity at y using the classical global resistance method, velocity is found to be proportional to h^E/n, where h is flow depth, and n is Manning's roughness. It is recognized that E = 2/3 for strict 1D straight flows. For compound channels, the parameter E needs a certain degree of reflection of the impact of turbulent diffusion between sub-sections. Cao et al. (2006) gave Equations (11) and (12) for the parameter E using Dr as the function of the model for the smooth and rough floodplain, respectively. The following models have been used to compute the overall stage-discharge for the multi-staged channel (see **Figure 7**).

$$E = 0.7987Dr^2 - 1.1955Dr + 0.5138 \tag{11}$$

$$E = -1.799Dr^2 - 0.0885Dr + 0.5704 \tag{12}$$

To test the performance of the models given by Cao et al. (2006) using the calibration of E for new configurations of staged compound channels, experimental data of smooth and rough floodplains are used, as shown in **Figure 7**. However, Equation (13) represents the best model for predicting stage-discharge for rough multi-stage channels. Furthermore, the depth ratio (Dr) in Equation (13) is calculated concerning the bankfull height of the stage two floodplain ($0 \geq y \geq 0.225$).

$$E = 0.1390Dr^2 - 0.1782Dr + 0.5899 \quad R^2 = 0.96 \tag{13}$$

Cao et al. (2006) model tested here shows a good agreement for predicting stage-discharge for lower depth ratio (Dr) of multi-staged asymmetric compound channel datasets used in the experimental study. However, indicated stage discharge using Equations (12) for the multi-stage channel (see **Figure 7**) is inconsistent with the experimental data for a higher depth ratio. Thus a new model is proposed for the multi-stage compound channel using the same approach proposed by Cao et al. (2006). The possible reason for the inconsistency of the model Equation (12) could be explained on the basis that for the flow depth over multi-stage floodplains when it increases above the bankfull level of the second stage, the fractional contribution of the main channel remains significant due to the presence of first stage floodplain. Thus, for the compound channel to act as a whole single channel, the b/H ratio has to be sufficiently low compared to the compound channels with single-stage channels.

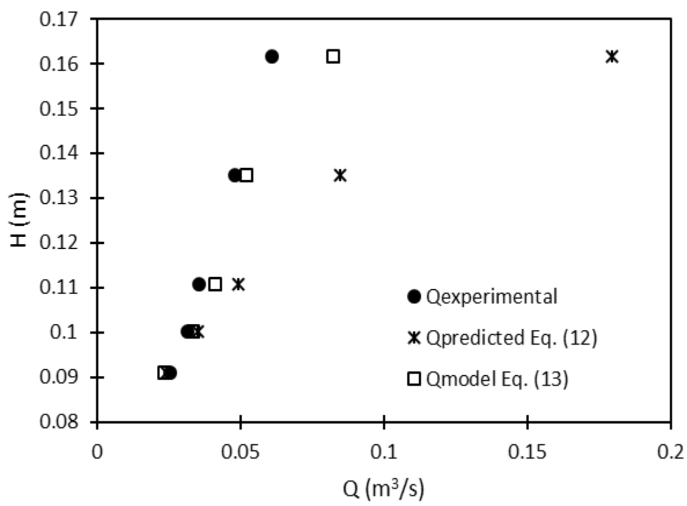

Figure 7. Prediction of stage discharge using parameter *E* calibrated by Cao et al. (2006) for staged floodplains.

5. Conclusion

Compound channels with multi-staged floodplain were tested with a uniform steady-state condition where the turbulent exchange process was investigated experimentally using ADV to understand the flow mechanism in these new configurations. Flow resistance tested for the new configuration shows that for the multi-stage channel, as the flow depth increases over the second stage floodplain, fractional contribution of the main channel and first stage floodplain under bankfull height still plays a pivotal role for higher depth ratio. Therefore, a new mathematical model has been suggested for estimating the zonal, overall and stage-discharge relationship for multi-stage channels using the 1D technique of overall roughness correction.

Acknowledgements

This work is partially supported by the National Natural Science Foundation of China (No. 11772270) and from the XJTLU research funds (KSF-E-17, RDF-16-02-02).

Conflicts of Interest

The authors declare no conflicts of interest regarding the publication of this paper.

References

Cao, Z., Meng, J., Pender, G., & Wallis, S. (2006). Flow Resistance and Momentum Flux in Compound Open Channels. *Journal of Hydraulic Engineering, 132,* 1272-1282. https://doi.org/10.1061/(ASCE)0733-9429(2006)132:12(1272)

Chen, G., Zhao, S., Huai, W., & Gu, S. (2019). General Model for Stage-Discharge Prediction in Multi-Stage Compound Channels. *Journal of Hydraulic Research, 57,* 517-533. https://doi.org/10.1080/00221686.2018.1494055

Huthoff, F., Roos, P. C., Augustijn, D. C., & Hulscher, S. J. (2008). Interacting Divided Channel Method for Compound Channel Flow. *Journal of Hydraulic Engineering, 134,* 1158-1165. https://doi.org/10.1061/(ASCE)0733-9429(2008)134:8(1158)

Proust, S., & Nikora, V. I. (2020). Compound Open-Channel Flows: Effects of Transverse Currents on the Flow Structure. *Journal of Fluid Mechanics, 885*. https://doi.org/10.1017/jfm.2019.973

Singh, P., & Tang, X. (2020). Zonal and Overall Discharge Prediction Using Momentum Exchange in Smooth and Rough Asymmetric Compound Channel Flows. *Journal of Irrigation and Drainage Engineering, 146,* 05020003. https://doi.org/10.1061/(ASCE)IR.1943-4774.0001493

Singh, P., Tang, X., & Rahimi, H. (2019). Study of Apparent Shear Stress and Its Coefficient in Asymmetric Compound Channels Using Gene Expression and Neural Network. *Journal of Hydrologic Engineering, 24*. https://doi.org/10.1061/(ASCE)HE.1943-5584.0001857

Tang, X. (2016). Critical Evaluation on Different Methods for Predicting Zonal Discharge of Straight Compound Channels. In Constantinescu, Garcia, & Hanes (Eds.), *River Flow 2016* (Vol. 1, pp. 51-64). Faylor & Francis. https://doi.org/10.1201/9781315644479-13

Tang, X. (2017). An Improved Method for Predicting Discharge of Homogeneous Compound Channels Based on Energy Concept. *Flow Measurement and Instrumentation, 57,* 57-63. https://doi.org/10.1016/j.flowmeasinst.2017.08.005

Tang, X. (2019a). A New Apparent Shear Stress-Based Approach for Predicting Discharge in Uniformly Roughened Compound Channels. *Flow Measurement and Instrumentation, 65,* 280-287. https://doi.org/10.1016/j.flowmeasinst.2019.01.012

Tang, X. (2019b). Apparent Shear Stress-Based Approach on an Inclined Interface Plane for Predicting Discharge in Straight Compound Channels. *MethodX, 6,* 1323-1330. https://doi.org/10.1016/j.mex.2019.05.027

Tominaga, A., & Nezu, I. (1991). Turbulent Structure in Compound Open-Channel Flows. *Journal of Hydraulic Engineering, 117,* 21-41. https://doi.org/10.1061/(ASCE)0733-9429(1991)117:1(21)

Wang, W., Huai, W. X., & Gao, M. (2014). Numerical Investigation of Flow through Vegetated Multi-Stage Compound Channel. *Journal of Hydrodynamics, 26,* 467-473. https://doi.org/10.1016/S1001-6058(14)60053-6

Yang, K., Liu, X., Cao, S., & Huang, E. (2014). Stage-Discharge Prediction in Compound Channels. *Journal of Hydraulic Engineering, 140,* 06014001. https://doi.org/10.1061/(ASCE)HY.1943-7900.0000834